JOURNAL OF MATERIALS SCIENCE 32 (1997) 4749–4758

Fracture mechanisms of poly(ethylene terephthalate) and blends with styrene-butadiene-styrene elastomers

V. TANRATTANAKUL, W. G. PERKINS*, F. L. MASSEY*, A. MOET§, A. HILTNER, E. BAER
Department of Macromolecular Science and Centre for Applied Polymer Research, Case Western Reserve University, Cleveland, OH 44106, USA
** Polyester Technical Centre, Shell Chemical Company, Akron, OH 44305, USA*
§ Department of Chemical and Petroleum Engineering, United Arab Emirate University, Al-Ain, UAE

Poly(ethylene terephthalate) (PET) was blended with 5 wt% of an elastomeric block copolymer. The hydrogenated styrene-butadiene-styrene (SEBS) elastomers were functionalized with 0–4.5 wt% maleic anhydride grafted on the midblock. Notched tensile tests in the temperature range −40–55 °C differentiated among the blends in terms of their toughness. The least effective elastomer was the unfunctionalized SEBS; all the functionalized SEBS elastomers effectively increased the toughness of PET. Fractographic analysis indicated that PET and the blend with unfunctionalized SEBS fractured through a pre-existing craze. Although adhesion of the unfunctionalized SEBS to the matrix was poor, the elastomer strengthened the craze somewhat, as indicated by an increase in length of the pre-existing craze when final separation occurred. A functionalized SEBS caused the fracture mechanism to change from crazing to ductile yielding. Graft copolymer formed by reaction of PET hydroxyl end groups with the anhydride *in situ* was thought to act as an emulsifier to decrease particle size and improve adhesion. These factors promoted cavitation, which relieved the triaxiality at the notch root and permitted the matrix to shear yield.

1. Introduction

Although poly(ethylene terephthalate) (PET) is tough in an unnotched situation, like other polar engineering thermoplastics it tends to be notch sensitive and stress concentrations can cause the fracture mode to change from ductile to brittle. It has been demonstrated that blending PET with small amounts of a functionalized styrenic block copolymer reduces notch sensitivity and significantly increases toughness [1, 2]. It is thought that a graft copolymer formed *in situ* by the reaction of PET hydroxyl end groups with grafted maleic anhydride acts as an emulsifier to promote dispersion of the elastomer in the melt and improve adhesion between the phases in the solid state.

The effectiveness of blending as a strategy for enhancing toughness relies on the promotion of alternative mechanisms of energy absorption [3]. The addition of a rubbery phase introduces the possibility of cavitational mechanisms that relieve the hydrostatic strain energy and enhance shear yielding of the matrix. This is generally thought to explain toughening of polar engineering thermoplastics in general and reduced notch sensitivity in particular [4, 5]. Additionally, dispersed particles act as a nucleating agent for uncrystallized PET to accelerate strain-induced crystallization and increase the fracture resistance of the yielded matrix [6].

Fractography is widely used in post-failure analysis to identify from the appearance of the fracture surface where the fracture originated, how it propagated, and whether it was ductile or brittle. The fracture surface of polymer blends, which represents the culmination of deformation and final separation, often provides clues to the role of the second phase [7]. In this study, a fractographic approach is used to gain insight into how the failure mechanisms change when PET is blended with an elastomer that enhances the toughness.

2. Experimental procedure

The PET provided by the Shell Chemical Company was Cleartuf® 7207, a bottle grade resin with an

Present address of V. Tanrattanakul: Polymer Science Program, Prince of Songkla University, Hat-Yai, Thailand.
All correspondence should be addressed to A. Hiltner.

0022–2461

intrinsic viscosity of 0.73 dl g^{-1}, molecular weights of $M_n = 24\,000$ and $M_w = 49\,000$, and a hydroxyl number of 1.4 mole per mole. Four hydrogenated styrene-butadiene-styrene (SEBS) elastomers with essentially the same composition and molecular weights were also provided by the Shell Chemical Company. The elastomers varied in the amount of grafted maleic anhydride, and are identified as SEBS-0MA (Kraton® G1652 without grafted anhydride), SEBS-1MA (Kraton® FG1921X with 1 wt % grafted anhydride), SEBS-2MA (Kraton® FG1901X with 2 wt % grafted anhydride), and SEBS-4.5MA (Kraton® B51-4 with 4.5 wt % grafted anhydride). The ratio of styrene to hydrogenated butadiene (EB) was 28 : 72 by weight, and the glass transition temperature of the EB block was $-42\,^{\circ}C$. The styrene equivalent molecular weights were approximately 75 000 (M_n) and 77 000 (M_w) for SEBS-0MA and SEBS-2MA, and 71 000 (M_n) and 73 000 (M_w) for SEBS-1MA and SEBS-4.5MA.

The components were dried and melt blended in a twin screw extruder as previously described [1, 2]. Blends with 5 wt % elastomer were processed with a barrel temperature of 280 °C and a screw speed of 35 r.p.m. The pellets were injection molded into a family mold that consisted of a 3.18 mm thick Type I tensile bar (ASTM D638), a 3.18 mm thick Izod impact bar (ASTM D256) and a 1.10 mm thick, 50 mm diameter disc using conditions previously described [1, 2]. The Izod bars were notched according to ASTM D256 with a 45° notch having a 0.25 mm radius and a 2.54 mm depth.

Tensile tests were performed on the notched Izod bars. The distance between grips was 50 mm and the crosshead speed was 500 mm min^{-1}. Tests were carried out at 55, 25, 0, -20 and $-40\,^{\circ}C$. Specimens were equilibrated in the Instron machine at the test temperature for 10 min before testing. Slower tensile tests were also made at ambient temperature using a crosshead speed of 0.1 mm min^{-1}. Some of these tests were interrupted before fracture in order to observe the damage zone at the notch root. Specimens from the interrupted tests were cut normal to the crack plane to obtain three sections of about the same thickness. The sections were polished and examined in the optical microscope. Fracture surfaces of all the specimens were coated with 9 nm of gold and examined in the Jeol 840A scanning electron microscope.

3. Results and discussion

3.1. Notched tensile behaviour

The stress–displacement curves of notched PET and blends with 5 wt % SEBS elastomer at three temperatures are shown in Fig. 1(a–c). These curves were obtained with the high extension rate, 500 mm min^{-1}. At 25 °C, the blends with an SEBS-g-MA all yielded at the notch root, in contrast to PET which fractured in a brittle manner. The blend with 5 wt % of unfunctionalized SEBS-0MA also fractured in a brittle manner but at a higher stress than PET. Tests at 0 °C differentiated between the blends with a functionalized elastomer: the blend with 5 wt % SEBS-4.5MA fractured in a brittle manner, the blend with 5 wt % SEBS-1MA remained ductile, and the blend with 5 wt % SEBS-2MA was intermediate. At $-20\,^{\circ}C$, all the compositions fractured in a brittle manner, but varied in the fracture stress or strain.

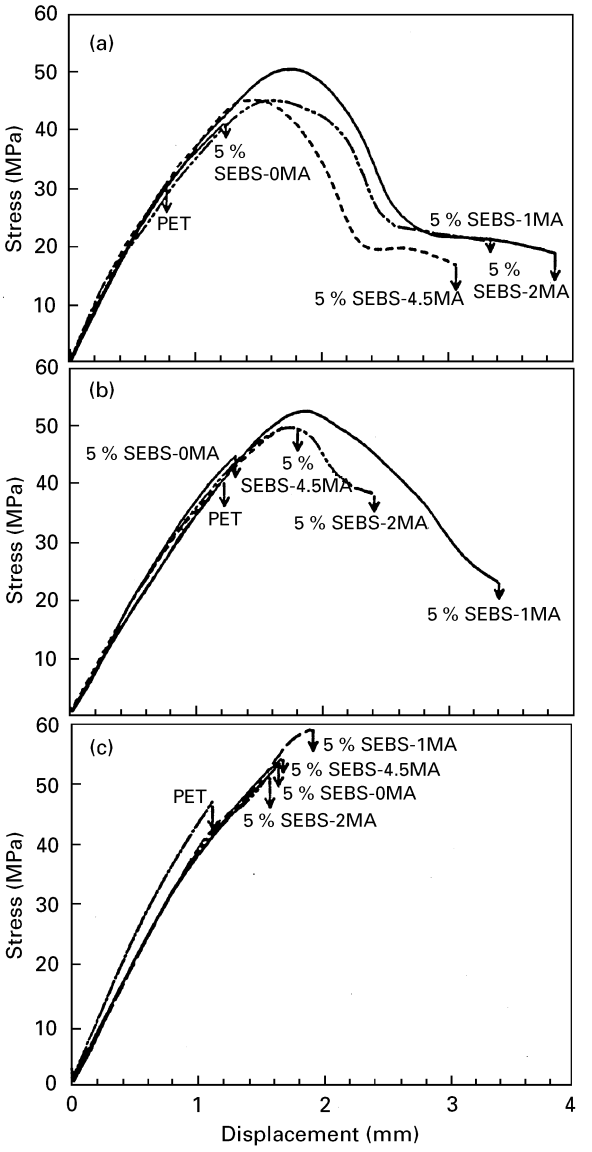

Figure 1 Stress–displacement curves of notched PET and blends with 5 wt % SEBS obtained with an extension rate of 500 mm min^{-1}. (a) 25 °C; (b) 0 °C; and (c) $-20\,^{\circ}C$.

The fracture energy, taken as the area under the stress–displacement curve, also differentiated among the blends, Fig. 2. The least effective elastomer was SEBS-0MA, it only slightly increased the fracture energy of PET. The striking difference between blends with SEBS-0MA and an SEBS-g-MA was attributed to the formation of an SEBS-g-PET copolymer which enhanced interfacial adhesion in the solid state and reduced the domain size by reducing interfacial tension in the melt state. The most effective was SEBS-1MA, the SEBS-g-MA with the lowest anhydride concentration. Increasing the functionality above 1 wt % produced a decrease in the fracture energy. The trend towards decreasing toughness with increasing functionality was credited to greater cavitation resistance as the particle size decreased [8].

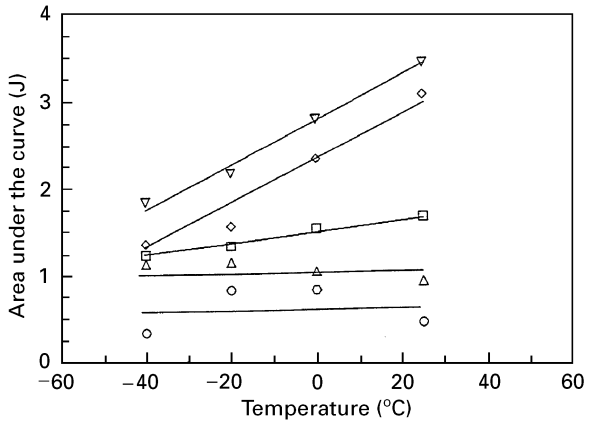

Figure 2 Temperature dependence of the fracture energy, taken as the area under the stress–displacement curve, for (○) PET, (△) 5 wt % SEBS-0MA, (□) 5 wt % SEBS-4.5MA (◇) 5 wt % SEBS-2MA and (▽) 5 wt % SEBS-1MA.

3.2. Fracture of PET

Notched PET also fractured in a brittle manner when tested at the low extension rate. Tensile tests performed at 25 °C with an extension rate of 0.1 mm min^{-1} were interrupted at two positions on the stress–displacement curve in order to examine the deformation at the notch root, Fig. 3(a–c). At position 1, two families of slip lines growing out from the notch formed a core yielding zone. At this position, the core yielding zone measured 54 μm in length. It increased slightly to 63 μm before a single thick craze initiated at the tip of the core yielding zone. As the craze lengthened, it took on a tapered shape. At position 2 on the stress–displacement curve the craze measured 385 μm in length and had opened up to about 20 μm at the tip of the core yielding zone where it initiated. The single craze continued to lengthen as the stress increased until the specimen fractured through the pre-existing craze.

Fracture surfaces showed a region of slow crack growth where the crack propagated through the pre-existing craze and a region of fast crack growth associated with catastrophic failure, Fig. 4(a–e). The slow crack growth region revealed that the pre-existing craze measured about 2 mm in length at fracture and had taken on a parabolic shape as it tunnelled into the centre of the specimen where the triaxiality was highest. The slow crack growth region exhibited several textures. Closest to the notch root where the crack speed was slowest, both fracture surfaces had the same cavitated texture with drawn out and torn craze fibrils (region A in Fig. 4a). About midway along the slow crack growth region the texture changed, and moreover was different on the two fracture surfaces. A ridged texture on the surface in Fig. 4a (region B) matched a relatively smooth featureless region on the other surface, Fig. 4b. Fig. 4c is a higher magnification micrograph of the ridged region shown in Fig. 4a. Numerous holes suggested the presence of crazed material underneath. Near the tip of the slow crack growth region of this specimen, the texture on the matching surfaces reversed. The transition from smooth to ridged texture in Fig. 4d shows the craze fibrils underneath the ridged surface. The texture in this region of slow crack growth resulted when final separation at the craze boundary left the entire craze on one of the surfaces.

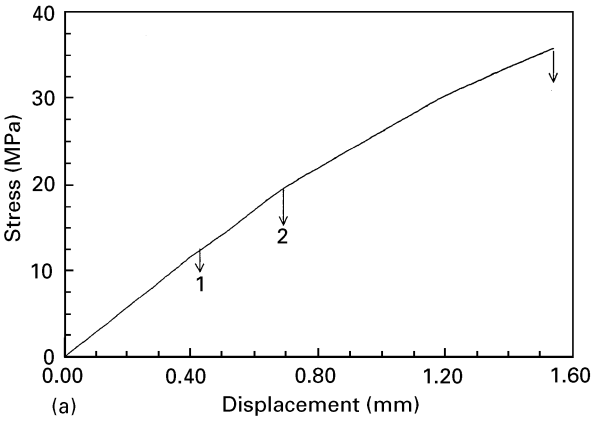

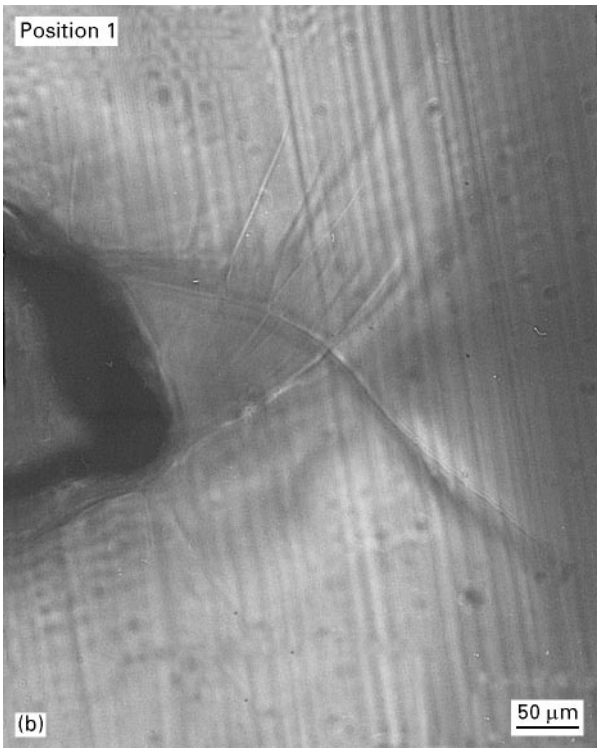

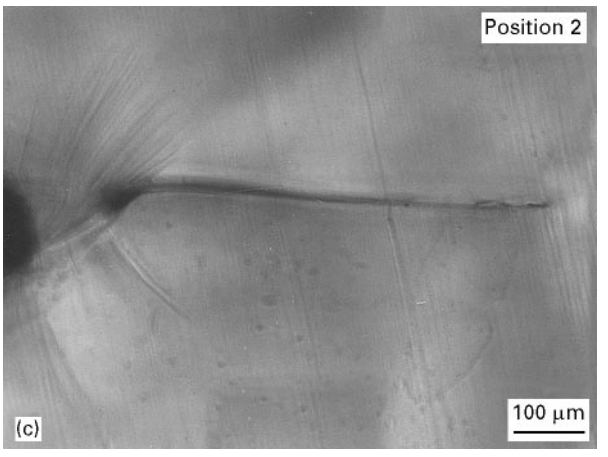

Figure 3 Notched tensile test of PET at 25 °C with a low extension rate of 0.1 mm min^{-1}. (a) The stress-displacement curve with optical micrographs of the notch root at: (b) position 1 and (c) position 2 on the stress–displacement curve.

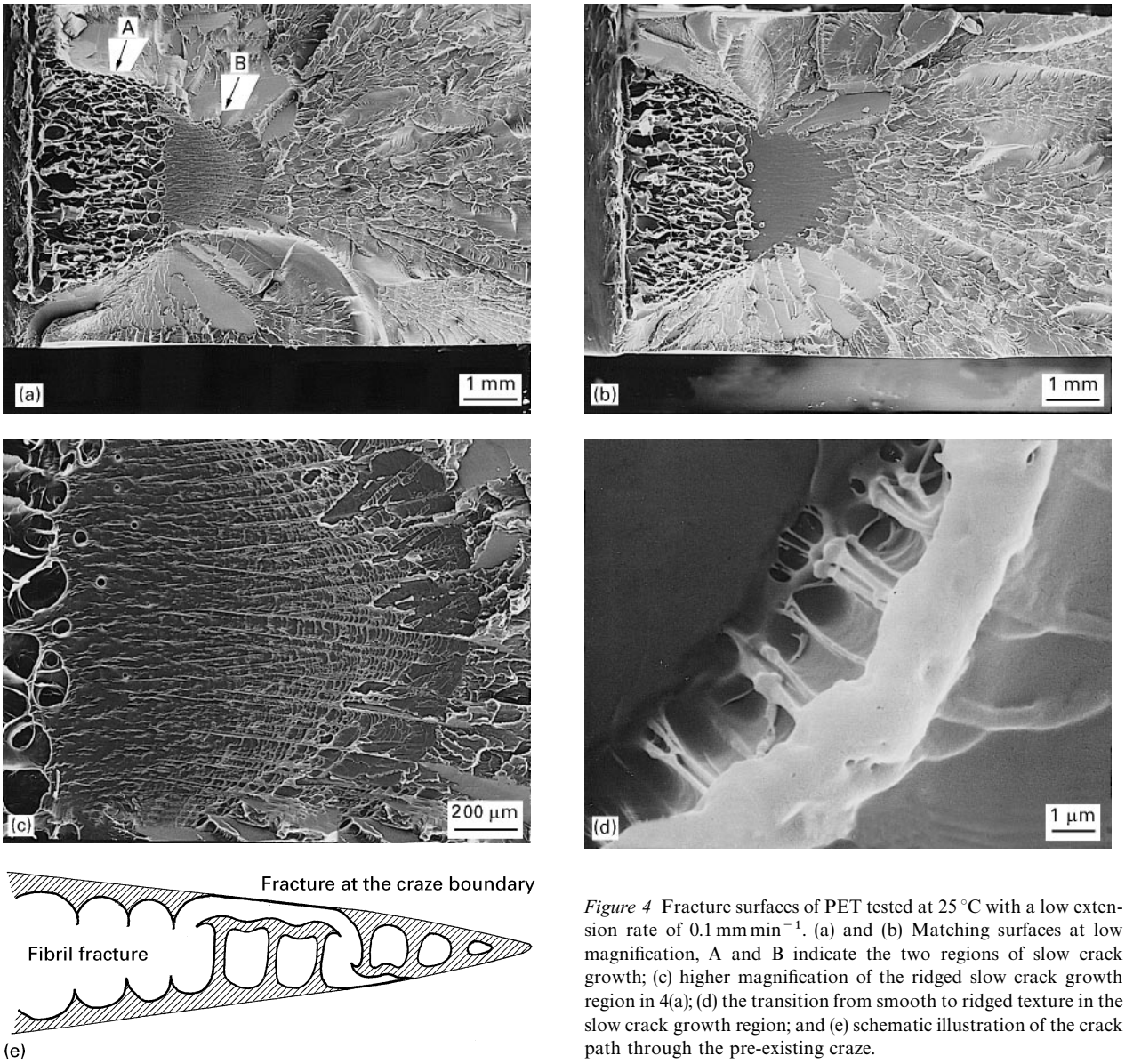

Figure 4 Fracture surfaces of PET tested at 25 °C with a low extension rate of 0.1 mm min^{-1}. (a) and (b) Matching surfaces at low magnification, A and B indicate the two regions of slow crack growth; (c) higher magnification of the ridged slow crack growth region in 4(a); (d) the transition from smooth to ridged texture in the slow crack growth region; and (e) schematic illustration of the crack path through the pre-existing craze.

The textures revealed how the crack path changed as the crack speed increased, Fig. 4e. Near the notch where the crack speed was slowest the crack propagated through the centre of the craze. Drawing and fracture of craze fibrils produced the same fibrillated texture on matching surfaces. As the crack speed increased, the crack path deviated to the interface between the craze and the surrounding bulk material. The underlying craze fibrils produced the characteristic ridges on the fracture surface that contained the craze.

This crack path is also typical of slow craze fracture in poly(styrene-acrylonitribe) (SAN) [9]. Differences in texture between craze fracture of "brittle" thermoplastics (SAN, polystyrene (PS) and polymethylmethacrylate (PMMA)) and craze fracture of PET result from the greater ductility of PET craze fibrils. The fractured fibrils in the region of slowest crack speed are more highly drawn in PET than on fracture surfaces of SAN, for example. In the region where the crack propagates between the crazed and uncrazed material, ridges on the PET surface reveal the underlying plastic deformation. In contrast, textural features on fracture surfaces of PS or PMMA, the so-called mackerel or patch patterns [10, 11], are produced by regular or irregular crack jumps from one side of the craze to the other. Otherwise these surfaces are smooth and featureless.

Brittle fracture in high-rate tests also started through a pre-existing craze as indicated by the matching fracture surfaces from a high-rate test at 55 °C, Fig. 5(a and b). Whereas the slow-rate, 25 °C fracture surface had two well-defined regions corresponding to fibril fracture and fracture at the craze boundary, the high-rate, 55 °C fracture surface exhibited more textures. There was only a small region near the notch root where drawn and fractured fibrils indicated that fracture occurred through the centre of the craze. Otherwise, fracture followed the craze boundary with numerous regions where the thin craze partially peeled away from the bulk material. Except for a few small regions, the craze remained on the surface in Fig. 5a and was detached from the surface in Fig. 5b. Fracture along the craze boundary produced a range of textures. Mostly, the craze interface fractured cleanly and both surfaces were smooth except for occasional ridges on the surface that

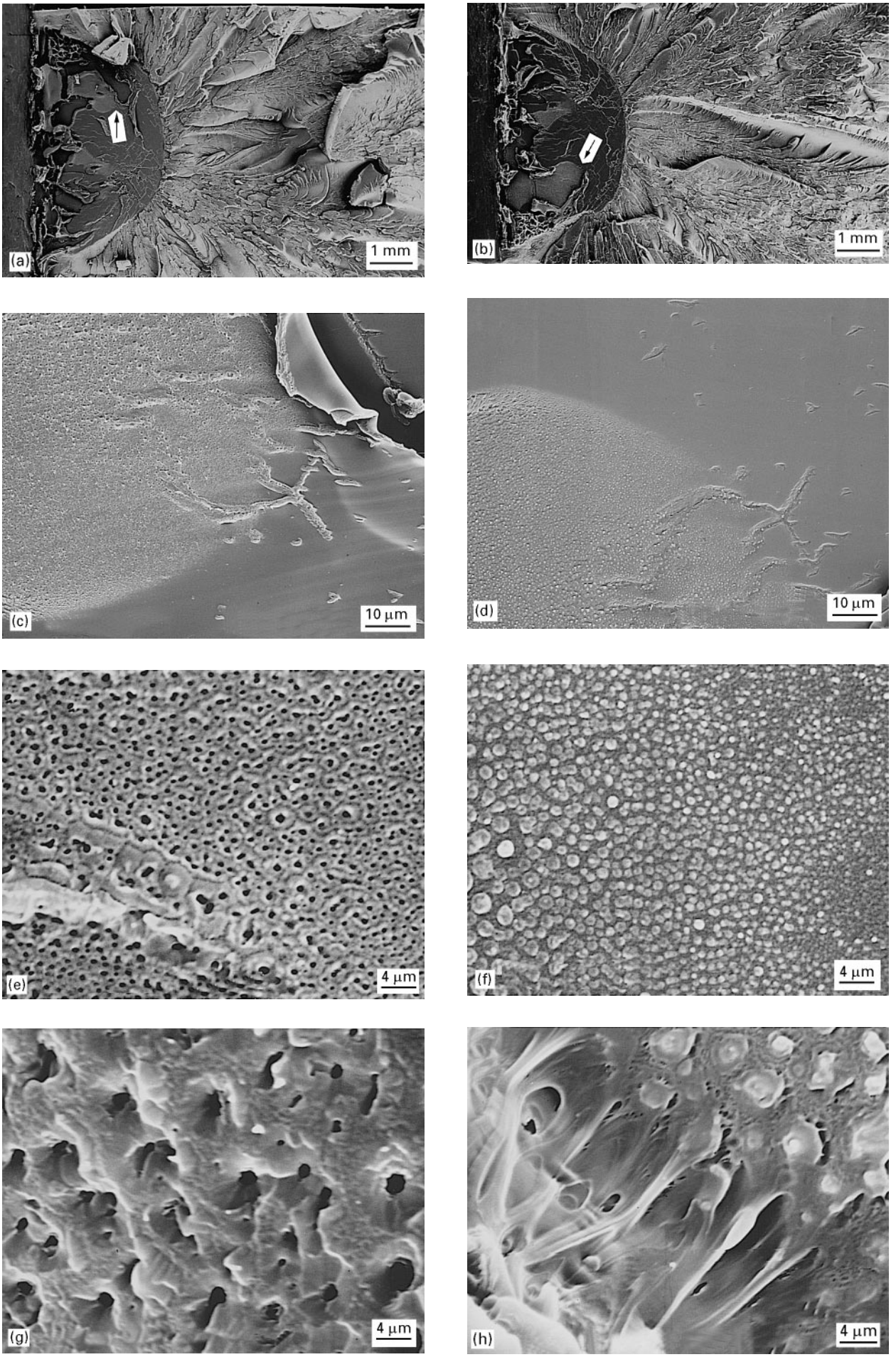

Figure 5 Fracture surfaces of PET tested at 55 °C with an extension rate of 500 mm min^{-1}. (a) and (b) Matching surfaces at low magnification; (c) and (d) higher magnifications of matching regions indicated by the arrows in 5(a) and 5(b), respectively; (e) and (g) from the textured region of 5(a) match (f) and (h) from 5(b).

contained the craze and matching fissures on the other surface. These textures are seen to the right in Fig. 5 (c and d).

There are two regions on the fracture surfaces in Fig. 5(a and b) where fracture at the craze boundary left a fine, overall texture: one region is near the centre of both surfaces and the other is closer to the top in Fig. 5a and the bottom in Fig. 5b. Fig. 5(c and d) are higher magnification micrographs of the matching regions indicated by the arrows in Fig. 5(a and b), respectively. They show the transition from the smooth surface further from the notch to the finely textured surface closer to the notch. The higher magnification micrographs of the textured region in Fig. 5(c and d) show that material pulled out along the craze interface leaving a porous texture on the surface that contained the craze, Fig. 5e, and a corresponding nodular texture on the matching surface, Fig. 5f.

In general, the texture reflected more plastic deformation of the craze boundary prior to final separation as the crack speed decreased and the fibrils in the underlying craze were more extended. The micrographs in Fig. 5(g and h) illustrate a region closer to the notch where the crack propagated more slowly. Fig. 5(e–h) all have the same magnification. Comparing Fig. 5(e and g), which are from the surface that contained the craze, the holes are much larger in Fig. 5g and are accompanied by more plastic deformation. The same is seen when the matching nodular structures, where the craze was detached, are compared in Fig. 5f and the upper right corner of Fig. 5h. Fig. 5h also includes a step where the crack path jumped from one craze boundary to the other. The exposed craze fibrils reveal the extent of plastic deformation that preceded fracture. In general, the textures reflect more plastic deformation of the craze fibrils before fracture, and more plastic deformation of the craze boundary during fracture as the crack speed decreased.

The characteristic texture with holes on the surface that contains the detached craze and nodules on the matching surface could result from the ability of PET fibrils to draw to high strains with strain hardening. Fig. 6 schematically illustrates a possible crack path during final separation along the craze boundary. The strain-hardened craze fibrils are strong enough that before they fracture, splits develop in the bulk material at the craze boundary. Microcracking near the craze boundary during fibril extension is suggested by Fig. 5h. Final separation occurs when the microcracks coalesce and the craze fibrils fracture. A hole remains on the surface that contains the detached craze and a fragment of the fractured craze fibril remains on the matching surface. Occasionally, instead of fracturing, the craze fibrils might pull out pieces of the bulk which would create the ridge/fissure combinations such as that in the centre right of Fig. 5(c and d).

The length of the pre-existing craze decreased with temperature to about 0.8 mm at 25 °C and less than 0.1 mm at − 20 °C. Fracture through the pre-existing craze at 25 °C left numerous steps where the crack passed from one craze boundary to the other. At higher magnification, the surfaces were smooth and featureless. The dominating texture on the fracture surface at − 20 °C was the hackle pattern. This texture characterizes fast fracture through craze bundles that form at the crack tip as the crack propagates [12].

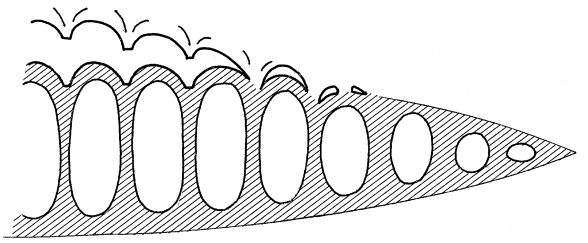

Figure 6 Schematic illustration of the crack path through the pre-existing craze in PET that would create holes on the surface with the craze and nodules on the matching surface.

3.3. Fracture of PET blended with unfunctionalized SEBS-0MA

The blend of PET with 5 wt % SEBS-0MA formed a single thick craze at the notch root in low-rate tests. In contrast to PET, there was no indication that crazing was preceded by formation of a core yielding zone at the notch root. Apparently the presence of the second phase reduced the critical stress for craze initiation enough that the craze condition was reached at the notch root before the shear yielding condition [4]. At an extension equivalent of position 1 on the stress–displacement curve in Fig. 3a, the blend had a single craze about 400 μm in length. Between positions 1 and 2, the craze lengthened from 400 to 800 μm. In comparison, the craze in PET initiated and grew to about 385 μm between positions 1 and 2.

The blend with 5 wt % SEBS-0MA exhibited macroscopically brittle fracture in high-rate tests at all temperatures. On the fracture surface, an area of stress-whitening that extended from the notch root indicated crack growth through the pre-existing craze. However, any plastic deformation associated with the stress-whitening was localized to the fracture plane because the stress-whitening was not visible on the side of the fractured specimen and there was no reduction of the cross-sectional area of the specimen. The stress-whitened area on matching fracture surfaces from a test at 55 °C are shown in Fig. 7(a and b). The pre-existing craze had grown to a length of about 3.5 mm when the blend fractured, about two and a half times the length of the pre-existing craze when PET fractured under the same conditions of temperature and rate. The surfaces did not show the drawn-out and torn fibrils that identified fracture through the centre of the craze. Instead, numerous steps with raised regions on one fracture surface, corresponding to depressed regions on the other, indicated that fracture followed the craze boundary.

Higher magnifications of a step showed raised regions on one surface and the matching depressed regions on the other, Fig. 7(c and d). The craze fibrils

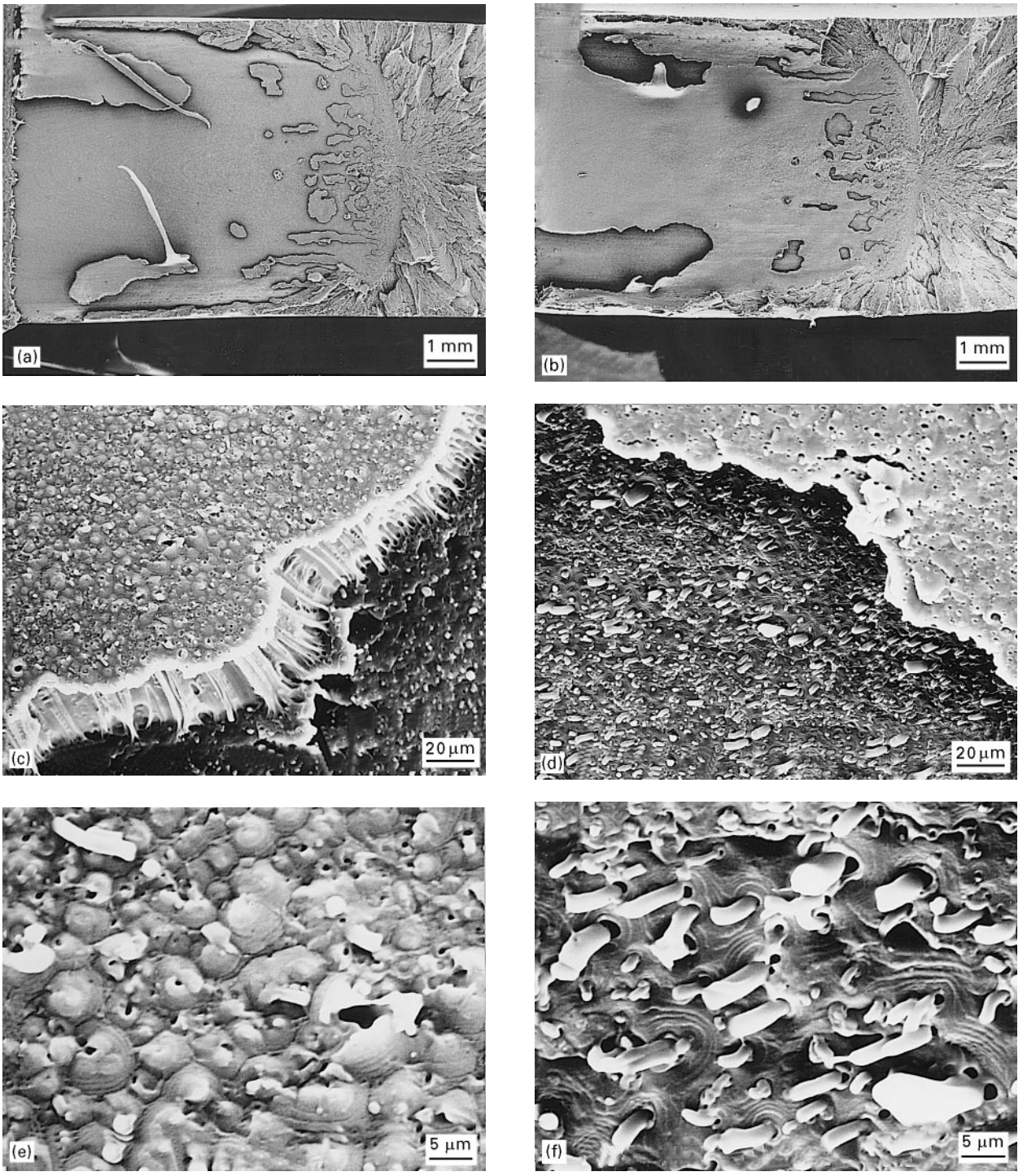

Figure 7 Fracture surfaces of PET with 5 wt % SEBS-0MA tested at 55 °C with an extension rate of 500 mm min^{-1}. (a), (c) and (e) Progressively higher magnifications of one fracture surface; and (b), (d) and (f) the corresponding regions of the matching fracture surface.

were revealed on the step where the fracture path passed from one craze boundary to the other. In the raised regions, i.e., regions that contained the underlying craze, the surface was characterized by numerous voids that were often surrounded by concentric wrinkles in the matrix, Fig. 7e. Occasionally a cylindrical segment of elastomer protruded from the surface. The matching depressed surface contained numerous cylindrical elastomer particles that corresponded to holes in the matching raised surface, Fig. 7f. The particles were also surrounded by concentric wrinkles in the matrix.

The cylindrical shape of the elastomer particles and their alignment in the injection direction were imparted by the flow field of the injection moulding process [2]. The way in which the specimens were subsequently notched and tested produced craze growth in the direction perpendicular to the elongated elastomer particles. As the matrix crazed, the elongated elastomer particles were also drawn out. Fig. 8 schematically illustrates the crack path through the pre-existing craze. During final separation, the crack path followed the craze boundary even at the notch root where the crack speed was slowest. Apparently the elastomer made it harder for the crack to follow a path through the centre of the craze, which would have required fracture of elastomer-reinforced craze

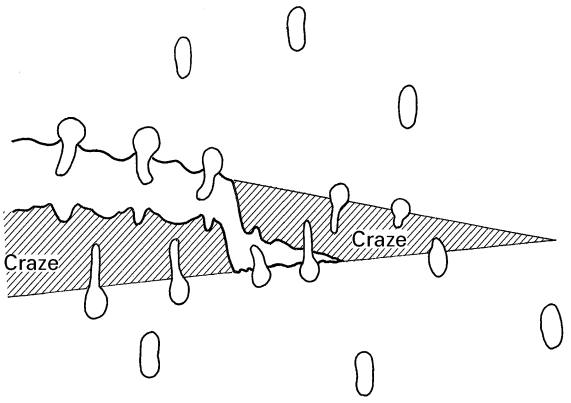

Figure 8 Schematic illustration of the crack path through the pre-existing craze in PET with 5 wt % SEBS-0MA.

fibrils, then to follow the craze boundary. As the crack followed the craze boundary, the elastomer particles generally pulled out rather than fractured. Pullout occurred preferentially from the crazed material, thus leaving holes on the raised surfaces and elastomer segments on the matching depressed surfaces. Retraction of the deformed matrix after fracture created the wrinkles.

Although the length of the slow crack propagation region decreased with test temperature, Fig. 9a, the predominant texture was the same at all temperatures: fracture along the craze boundary produced raised regions on one surface that matched depressed regions on the other. However, at the lower temperatures, there was less deformation of the matrix, and the elastomer particles did not appear to pull out preferentially from one side of the craze boundary. A higher magnification micrograph obtained from a 0 °C fracture surface shown in Fig. 9b shows the pulled-out elastomer particles and holes left by pulled-out particles that characterized both raised and depressed regions of the fracture surface. Compared to the 55 °C fracture, considerably less wrinkling of the matrix indicated that the matrix was not as highly drawn out before it fractured.

Test temperatures of 25 °C or lower produced one feature that was not observed in the 55 °C fracture. Groups of impinging irregular markings, or isolated circular markings, indicated where secondary cracks initiated within the pre-existing craze and propagated through the crazed material until they impinged on the primary crack or another secondary crack. These secondary cracks initiated at flaws within the craze, possibly created by large elastomer particles. The plane of the secondary cracks was intermediate between the craze boundaries as defined by the raised and depressed regions on the fracture surface. The texture in these regions was characterized by profuse cavitation and localized tearing fracture of the craze fibrils, and was identical on both fracture surfaces.

The slow crack growth region was always longer in the blend with SEBS-0MA than in PET tested under the same conditions. Even though adhesion of SEBS-0MA to the matrix was poor [2], apparently the elastomer strengthened the craze somewhat, as indicated by the increased length of the pre-existing craze when final separation occurred. The effect was enhanced by the alignment of the elongated elastomer particles in the direction perpendicular to the craze. This strengthening of the craze was manifested in a slight improvement of the toughness. Although fracture of the blend was characterized as brittle, the increased fracture stress and strain compared to PET resulted in a slightly higher fracture energy.

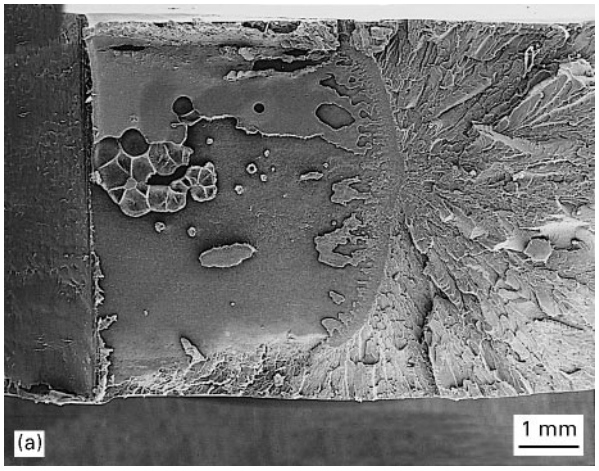

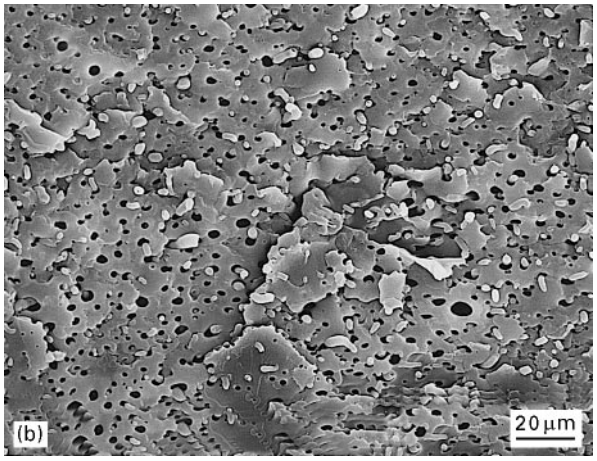

Figure 9 Fracture surfaces of PET with 5 wt % SEBS-0MA tested with an extension rate of 500 mm min^{-1}. (a) Tested at 25 °C; and (b) higher magnification of the slow crack growth region tested at 0 °C.

3.4. Fracture of PET blended with functionalized SEBS-g-MA

Blends of PET with an SEBS-g-MA were macroscopically ductile in high-rate tests at 55° and 25 °C. The fracture surface exhibited plane stress tearing fracture with considerable reduction in the cross-sectional area, Fig. 10a. The surface was entirely stress-whitened, and the stress-whitening extended some distance away from the fracture plane. At higher magnification, the fracture surface exhibited profuse cavitation and pull-out of matrix ligaments, Fig. 10b. The blended SEBS-g-MA particles were smaller and primarily spherical in contrast to the larger, highly elongated particles of SEBS-0MA. Good adhesion of the smaller particles to the matrix promoted particle cavitation, and caused the pre-fracture damage mechanism to change from

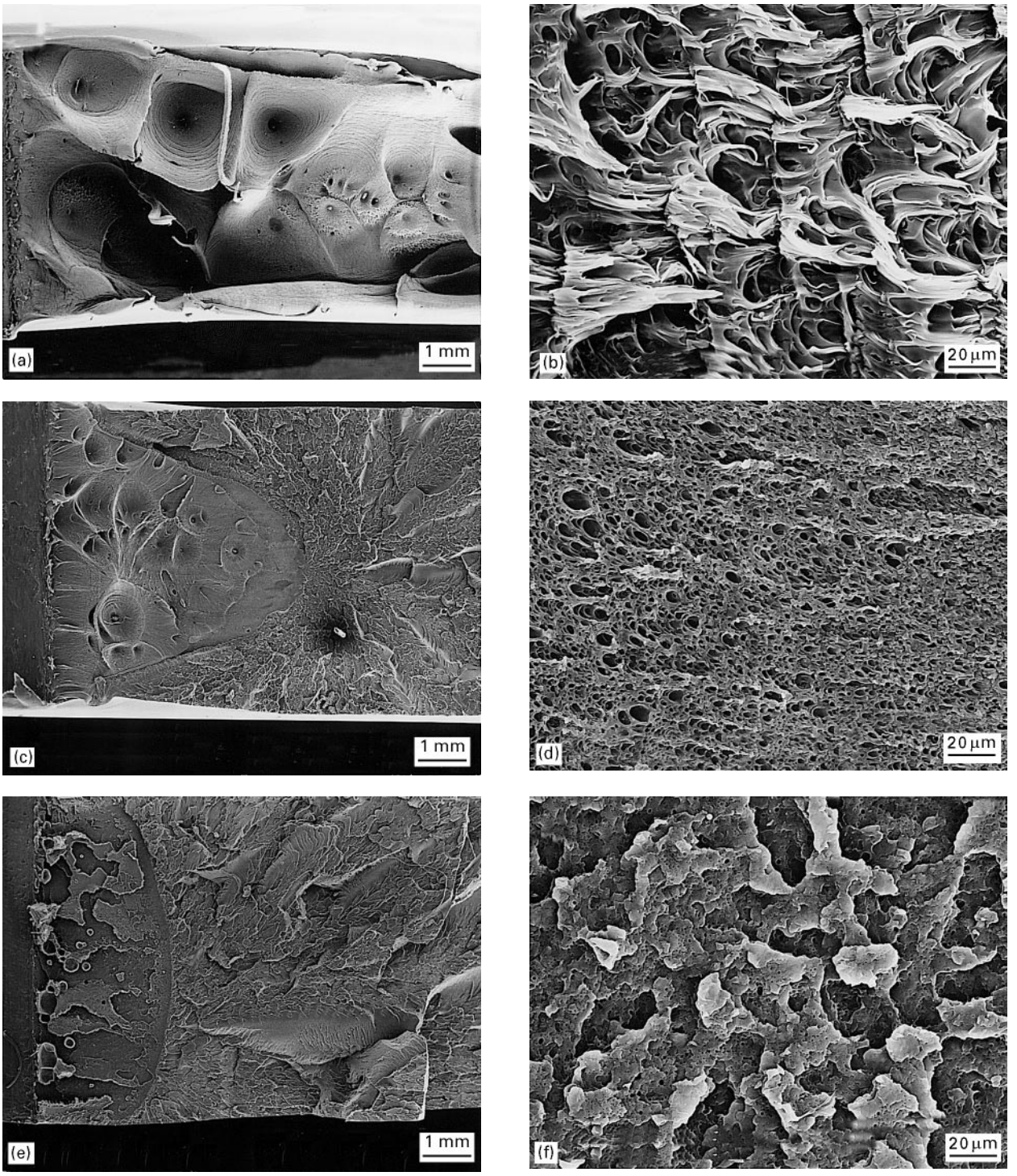

Figure 10 Fracture surfaces of PET blended with 5 wt % SEBS-4.5MA tested at 500 mm min^{-1}. (a) and (b) Tested at 25 °C; (c) and (d) tested at 0 °C; (e) and (f) tested at − 20 °C.

crazing to cavitation. Cavitation of the particles relieved the triaxiality at the notch root and enabled the matrix to shear yield. Subsequent fracture occurred by plane stress ductile tearing through a pre-existing plastic zone, rather than through a pre-existing craze.

The appearance of the fractured specimens suggested a damage zone similar to that described in toughened polycarbonate [13] and other rubber-toughened engineering plastics [14–17]. As indicated schematically in Fig. 11a, the damage zone might consist of two regions: a zone of intense stress whitening adjacent to the fracture plane and a larger zone of more diffuse stress whitening extending some distance from the fracture plane. Profuse particle voiding accompanied by plastic deformation of the matrix characterizes the intense zone; voiding without significant matrix deformation describes the diffuse zone. Because most of the pre-fracture deformation energy is absorbed by plastic deformation rather than void formation, the apparent toughness of a blend depends primarily on the characteristics of the intense zone [13].

At 0 °C blends with SEBS-1MA and SEBS-2MA showed yielding in the stress–displacement curves, in contrast to the blend with SEBS-4.5MA which fractured when it was close to the maximum stress. Correspondingly, fracture surfaces of SEBS-1MA and

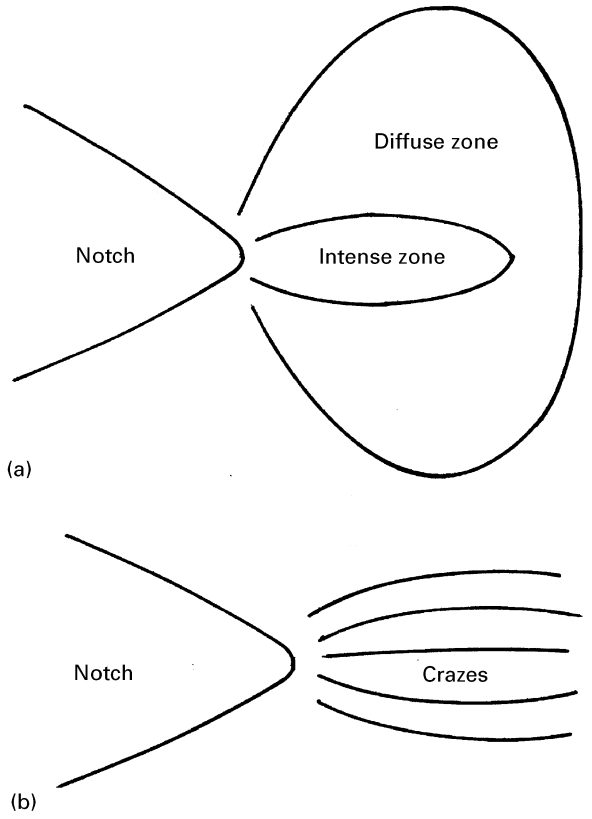

Figure 11 Schematic illustrations of the pre-fracture damage zone in blends of PET with SEBS-g-MA: (a) The plastic zone that precedes ductile fracture; and (b) the crazed zone.

SEBS-2MA blends were completely ductile, in contrast to the fracture surface of the SEBS-4.5MA blend which exhibited a region of ductile fracture at the notch root, and elsewhere the features of brittle fracture, Fig. 10c. Higher magnification of a region near the tip of the ductile region, Fig. 10d, showed cavitation and tearing although the extent of deformation was considerably less than in completely ductile fractures. The lower ductility of the SEBS-4.5MA blend, compared to SEBS-1MA and SEBS-2MA blends, was attributed to the smaller particle size and correspondingly greater cavitation resistance.

At -20° and $-40\,^{\circ}$C the fracture surfaces of all the SEBS-g-MA blends were the same. A very small region of cavitation and ductile tearing extended approximately 200–500 μm from the notch root; this was followed by a much larger region of slow crack growth with characteristics of craze fracture, and finally by a region of fast fracture with a hackle-like texture, Fig. 10e. The slow crack growth region was characterized by irregular step jumps where the crack might have jumped from one boundary of a craze to the other. These surfaces also contained occasional groups of impinging irregular markings, or isolated circular markings, that indicated secondary crack initiation within a pre-existing craze. However, because the features of craze fracture were not as well defined as on the fracture surfaces of PET or the SEBS-0MA blend, the pre-existing deformation might be described more accurately as a crazed zone or as multiple crazing, shown schematically in Fig. 11b. At higher magnification, the surfaces were very rough with no evidence of cavitation; instead there were numerous holes about the size of the elastomer particles, 0.5 μm or less, Fig. 10f. The test conditions of rate and temperature were too severe for particle cavitation, however the elastomer particles might have acted as crack deflectors to cause the surface roughness.

4. Conclusions

Fractography was used to identify the failure modes of PET and PET blends, and to characterize the brittle-to-ductile transition. Crazing was found to be the principal deformation mechanism of notched PET under all examined testing conditions of temperature and rate. This resulted in brittle fracture. Blending was examined as a strategy for promoting alternative mechanisms of energy absorption that would enhance the toughness. A small amount (5 wt %) of unfunctionalized SEBS-0MA was not effective in changing the deformation mechanism. Although the unfunctionalized elastomer strengthened the craze somewhat, the blend fractured in a brittle manner. Blending with a functionalized SEBS-g-MA introduced a cavitational mechanism that relieved the hydrostatic strain energy at the notch and enhanced shear yielding of the matrix. As a result, the fracture mechanism changed from crazing to ductile yielding.

Acknowledgement

The generous financial support of the Shell Chemical Company is gratefully acknowledged.

References

1. V. TANRATTANAKUL, W. G. PERKINS, F. L. MASSEY, A. MOET, A. HILTNER and E. BAER, *Polymer* (in press).
2. *idem*, *ibid.* (in press).
3. I. WALKER and A. A. COLLYER, in "Rubber toughened engineering plastics", edited by A. A. Collyer (Chapman & Hall, London, 1994) p. 29.
4. C. CHENG, A. HILTNER, E. BAER, P. R. SOSKEY and S. G. MYLONAKIS, *J. Appl. Polym. Sci.* **52** (1994) 177.
5. *idem*, *J. Mater. Sci.* **30** (1995) 587.
6. D. L. WILFONG, A. HILTNER and E. BAER, *ibid.* **21** (1986) 2014.
7. M.-P. LEE, A. HILTNER and E. BAER, *Polym. Engng. Sci.* **32** (1992) 909.
8. D. DOMPAS, G. GROENINCKX, M. ISOGAWA, T. HASEGAWA and M. KADOKURA, *Polymer* **35** (1994) 4750.
9. E. S. SHIN, A. HILTNER and E. BAER, *J. Appl. Polym. Sci.* **46** (1992) 213.
10. J. MURRAY and D. HULL, *J. Polym. Sci. A-2* **8** (1970) 583.
11. M. J. DOYLE, *J. Mater. Sci.* **17** (1982) 204.
12. W. DÖLL, in "Fractography and failure mechanics of polymers and composites", edited by A. C. Roulin-Moloney (Elsevier Applied Science, London, 1989) p. 387.
13. C. CHENG, N. PEDUTO, A. HILTNER, E. BAER, P. R. SOSKEY and S. G. MYLONAKIS, *J. Appl. Polym. Sci.* **53** (1994) 513.
14. C. J. CHOU, K. VIJAYAN, D. KIRBY, A. HILTNER and E. BAER, *J. Mater. Sci.* **23** (1988) 2533.
15. H.-J. SUE and A. F. YEE, *ibid.* **24** (1989) 1447.
16. M. C. M. van der SANDEN and H. E. MEIJER, *Polymer* **35** (1994) 2774.
17. K. DIJKSTRA, J. ter LAAK and R. J. GAYMANS, *ibid.* **35** (1994) 315.

Received 8 October 1996
and accepted 10 February 1997